ADVANCED MATERIALS
www.advmat.de

Incorporating Flexibility into Stiffness: Self-Grown Carbon Nanotubes in Melamine Sponges Enable A Lithium-Metal-Anode Capacity of 15 mA h cm^{-2} Cyclable at 15 mA cm^{-2}

*Jian Xie, Jianglin Ye, Fei Pan, Xuemei Sun, Kun Ni, Hong Yuan, Xiangyang Wang, Na Shu, Chunhua Chen, and Yanwu Zhu**

Although with an extremely high theoretical capacity (3860 mA h g^{-1}), the lithium (Li) metal anodes reported so far typically possess capacities of ≤5 mA h cm^{-2} and cyclable at currents of ≤5 mA cm^{-2}. In this work, a hierarchal carbon scaffold is designed with the self-growth of carbon nanotubes (CNTs) in nickel-decorated melamine sponges via thermal annealing. It is found that the nitrogen-doped carbon obtained from the melamine sponge, coupled with CNTs, provides an overall strong yet internally flexible host which enables an areal capacity of up to 15 mA h cm^{-2} cyclable at a charging/discharging current of 15 mA cm^{-2} as Li metal anodes. Characterizations show that the highly conductive yet uniformly distributed CNTs effectively suppress the local current density, leading to more uniform Li nucleation in Li plating. The flexible CNTs in the stiff scaffold enhance the tolerance to the stress caused by the intrinsic volume variation in Li plating/striping, resulting in the stable cycling performance at high currents. This study provides a potentially scalable and cost-effective strategy for preparation of high-performance Li-metal anodes.

Conventional graphite anodes for lithium (Li) ion batteries cannot meet the high-energy-density demand because of the limited capacity of 372 mA h g^{-1}. Alternatively, metallic Li has retriggered a huge research interest as a candidate for anodes owing to the appealing features including extremely high theoretical capacity (3860 mA h g^{-1}), very low reduction potential (−3.04 V vs standard hydrogen electrode), and low density (0.534 g cm^{-3}).[1,2] Li-metal batteries, such as Li-sulfur and Li-air batteries, have revived considerable attention.[3,4] However, unlike graphite or silicon anodes that host Li ions by forming Li-intercalated compounds, Li-metal anodes store energy by plating/stripping of Li across the Li/electrolyte interface, leading to a nearly infinite relative dimensional change (e.g., a capacity of 10 mA h cm^{-2} requires plating/stripping of 50 µm thick Li). The large volume variation brings cracks in the solid electrolyte interphase (SEI) and thus results in unstable SEI, which deteriorates the Coulombic efficiency as well. Subsequently, the fresh Li underneath the cracked SEI is exposed to electrolyte, lowering the energy barrier for Li-ion transport; the enhanced ion flux through cracks further intensifies nonuniform Li deposition.[3,5–8] Besides, the uneven surface of conventional Li-on-Cu (Li@Cu) electrode induces the nonuniform distribution of electric field and thus the inhomogeneous charge distribution; the adsorption of Li ions on the tips of protrusions has led to a commonly known "tip effect".[9] The high local electric field and concentrated Li ions expedite the nucleation and growth of metallic Li, which gradually evolves into Li dendrites.[10] These issues have caused significant problems related to cycle life and safety when the Li metal is used as anode.

Considerable effort has been devoted to overcoming these problems. One strategy focuses on the design of SEI layer to stabilize the anode/electrolyte interface, which typically includes i) optimizing electrolyte contents,[11–13] ii) engineering solid electrolytes,[14,15] and iii) employing an artificial SEI.[16,17] These designs modify the properties of SEI and hinder the breaking, thus improving the Coulombic efficiency and inhibiting the development of Li dendrites.[2] Another strategy is to optimize the electrode for more homogeneous Li deposition, which often takes advantages of increased electrode/electrolyte interface[18,19] and doping.[20,21] The former is based on Sand's law in which the time (τ) needed for Li dendritic growth follows a power law as a function of the current density (J)

$$\tau = \pi D \left(\frac{eC_0}{2J}\right)^2 \left(\frac{\mu_a + \mu_c}{\mu_a}\right)^2 \quad (1)$$

J. Xie, J. Ye, F. Pan, X. Sun, K. Ni, H. Yuan, X. Wang, N. Shu, Prof. C. Chen, Prof. Y. Zhu
Hefei National Research Center for Physical Science at the Microscale
CAS Key Laboratory of Materials for Energy Conversion & Department of Materials Science and Engineering
University of Science and Technology of China
Hefei, Anhui 230026, P. R. China
E-mail: zhuyanwu@ustc.edu.cn
Prof. Y. Zhu
iChEM (Collaborative Innovation Center of Chemistry for Energy Materials)
University of Science and Technology of China
Hefei, Anhui 230026, P. R. China
The ORCID identification number(s) for the author(s) of this article can be found under https://doi.org/10.1002/adma.201805654.

DOI: 10.1002/adma.201805654

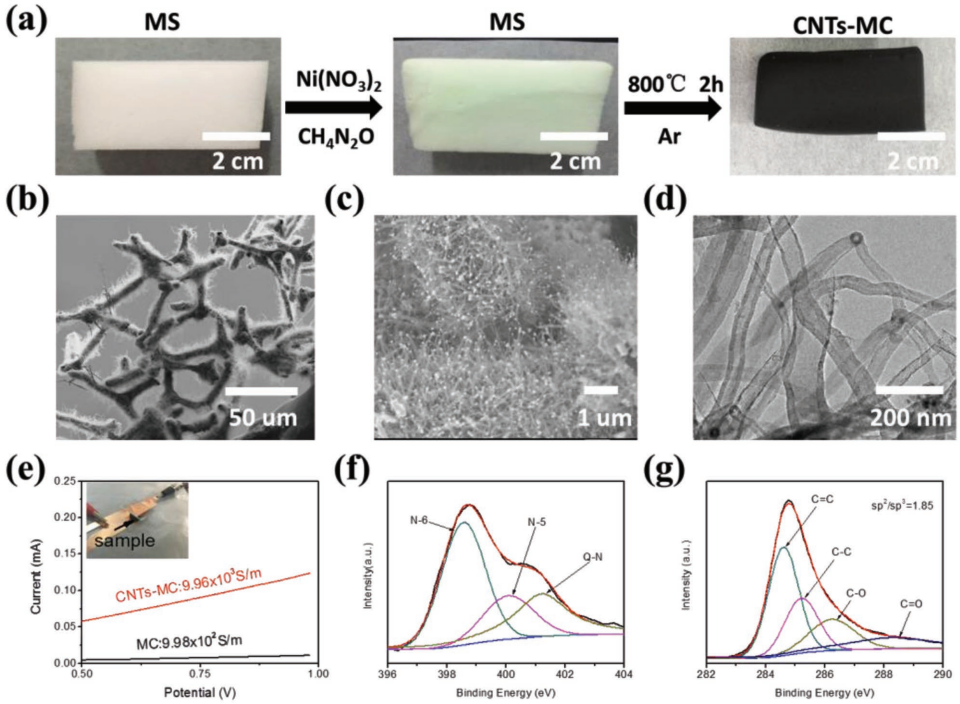

Figure 1. a) Procedures and corresponding optical images for the preparation of CNTs-MC. b,c) Typical SEM images and d) TEM image of CNTs-MC. e) *I–V* curves of CNTs-MC and MC measured using the two-electrode setup shown in the inset. f) XPS N 1s and g) C 1s spectra of CNTs-MC.

where D is the ambipolar diffusion coefficient, e the electron charge, C_0 the electrolyte concentration, μ_a and μ_c the anionic and cationic mobility, respectively. Therefore, the higher electrode/electrolyte interface area typically leads to the smaller local current on the anode surface and consequently longer deposition time that postpones the nucleation of Li dendrites. In terms of doping effect, theoretical calculations show that the matrix with nitrogen (N)-[20] or oxygen (O)-containing[22] functional groups has stronger interactions with Li atoms, which would guide more uniform nucleation of Li. For instance, it was reported that the N-containing groups in graphitic carbon sponges resulted in homogenous Li nucleus and the Li seed layer regulated a well-distributed Li growth in the following process.[23] Moreover, a 3D porous structure has been proved to reduce the overall volume change of electrodes during Li plating/stripping.[19,24,25]

Although the proceedings mentioned above, most Li-metal anodes reported are limited with the charging/discharging current of ≤5 mA cm^{-2} (for capacities ≥5 mA h cm^{-2})[8,23,24,26] and the capacity of ≤5 mA h cm^{-2} (for currents ≥5 mA cm^{-2}).[10,27–32] High-performance Li-metal batteries prefer a capacity of ≈10 mA h cm^{-2} or higher[33] which should be able to work at high currents as well. For example, it was reported that a sulfur cathode exhibited a high specific capacity of 920 or 548 mA h g^{-1} after 200 cycles measured at 2 C (7.9 mA cm^{-2}) or 4C (15.8 mA cm^{-2}), respectively.[34] Thus, developing Li-metal hosts with ability of achieving simultaneously high capacity and high current is desired. To achieve such a performance, a 3D carbon with a stiff structure to maintain the stable SEI, yet with mechanisms to homogenize the Li deposition and to adsorb the internal strain shall be finely tailored.

Herein, we report the preparation of carbon nanotubes (CNTs)-decorated carbon sponges by simply heating melamine sponges (noted as MSs) loaded with nickel particles. The obtained carbon (noted as CNTs-MC) consists of flexible CNTs grown on the relatively stiff graphitic scaffolds without needing any other carbon sources. The melamine naturally provides N- and O-containing functional groups in CNTs-MC. When the CNTs-MC is electrodeposited with Li as a Li-metal anode, it demonstrates a Coulombic efficiency of ≈98% at the current of 10 mA cm^{-2} for the capacity of 10 mA h cm^{-2}. More impressively, the anode is cyclable at a current density of 15 mA cm^{-2} for a high capacity of up to 15 mA h cm^{-2}. Detailed characterizations show that the combination of stiff scaffold and flexible CNTs assures the excellent structural stability in cycling, revealed by a relatively small electrode thickness change at 10 mA cm^{-2} for 10 mA h cm^{-2} and more efficient energy adsorption in the deformation of electrodes.

The preparation procedure of CNTs-MC is briefly illustrated in the **Figure 1**a and the detailed experimental description is provided in Supporting Information. To obtain CNTs-MC, a melamine sponge (MS) was thoroughly soaked with $Ni(NO_3)_2$ (as catalyst precursor[35]) and urea (to help the homogeneous growth of CNTs, see Figure S1, Supporting Information) before annealing at 800 °C for 2 h in argon (Ar). Decreasing the amount of $Ni(NO_3)_2$ or the flow of Ar has caused sparser growth of CNTs on MC (Figure S1c,e, Supporting Information). Heating duration has also been optimized to maintain the complete structure of MC (Figure S1d,f, Supporting Information). Bare MC was also prepared as a control by processing MS at the same annealing conditions but without introducing $Ni(NO_3)_2$. After annealing, the CNTs-MC appears a black,

freestanding chunk which can be picked up by tweezers. The scanning electron microscopy (SEM) image in Figure 1b shows that the CNTs-MC contains interconnected scaffolds, similar to that in MS or MC (Figure S2, Supporting Information). The higher magnification SEM image in Figure 1c shows the bunch of CNTs with nanoparticles on the tip, which might indicate a tip-growth mechanism[35]; the X-ray photoelectron spectroscopy (XPS) Ni 2p spectrum of CNTs-MC (Figure S3a, Supporting Information) reveals that the nanoparticles are NiO. The transmission electron microscopy (TEM) image (Figure 1d) shows the tubular structure of multiwalled CNTs which may have open tips or are interconnected by the particles. By counting one hundred randomly distributed CNTs, the average outer diameter is estimated as ≈60.2 nm obtained in the range of from 1 to 160 nm (Figure S3c, Supporting Information). By counting ten high-resolution TEM (HRTEM) images (Figure S3b, Supporting Information), the wall thickness of CNTs falls is 2.5–14.8 nm, corresponding to ≈7–43 graphitic layers. Energy disperse spectroscopy (EDS) shows the homogenous dispersion of C, O, and N in the skeleton of CNTs-MC (Figure S4, Supporting Information). The X-ray diffraction (XRD) patterns (Figure S5a, Supporting Information) show broad peaks at ≈25.2°, corresponding to the (002) interlayer distance of graphitic carbon. The Raman spectra (Figure S5b, Supporting Information) show that CNTs-MC and bare MC contain plenty of defects or amorphous carbon. The Fourier transform infrared spectroscopy (FTIR) spectra (Figure S5c, Supporting Information) demonstrate that CNTs-MC and bare MC contain O—H (3453 cm^{-1}) and C=N (1605 cm^{-1}) groups.[36] The XPS survey spectrum (Figure S5d, Supporting Information) shows that the CNTs-MC contains elements of C (77.94 at%), N (12.04 at%), O (7.64 at%), Ni (1.93 at%). The CNTs-MC presents an electrical conductivity of ≈9.96×10^3 S m^{-1}, one order higher than the bare MC (≈9.98×10^2 S m^{-1}), as shown by the two-electrode electric measurement curves in Figure 1e. The CNTs-MC has a mass density of ≈0.017 g cm^{-3}, specific surface area (SSA) of ≈408 m^2 g^{-1} (Figure S5e, Supporting Information), pore volume of ≈0.254 cm^3 g^{-1} (Figure S5f, Supporting Information); the porosity is ≈99%, suggesting that a 100 µm thick CNTs-MC theoretically can accommodate 99 µm thick Li, namely a theoretical capacity of 19.8 mA h cm^{-2}. The XPS N 1s spectrum of CNTs-MC (Figure 1f) can be deconvoluted into peaks of pyridine nitrogen (N-6, ≈398 eV), pyrrolic nitrogen (N-5, ≈400 eV), and quaternary nitrogen (Q-N, ≈401 eV).[37] The XPS C 1s spectrum (Figure 1g) shows the existence of C=O and C—O, consistent with FTIR results. The sp^2/sp^3 ratio of CNTs-MC (1.85) is higher than MC (1.69) estimated by XPS, probably due to the existence of CNTs and/or the catalytic role of Ni.

The Coulombic efficiency of CNTs-MC has been compared to that of Cu foils via galvanostatic discharge/charge profiles. As shown in **Figure 2**a, when 5 mA cm^{-2} is applied to electroplate Li on the CNTs-MC for 1 h, corresponding to a Li content of 27.2 wt% in Li@CNTs-MC, the Coulombic efficiency is measured as 86.7%, 96.7%, 95%, or 90% for the 1st, 5th, 20th,

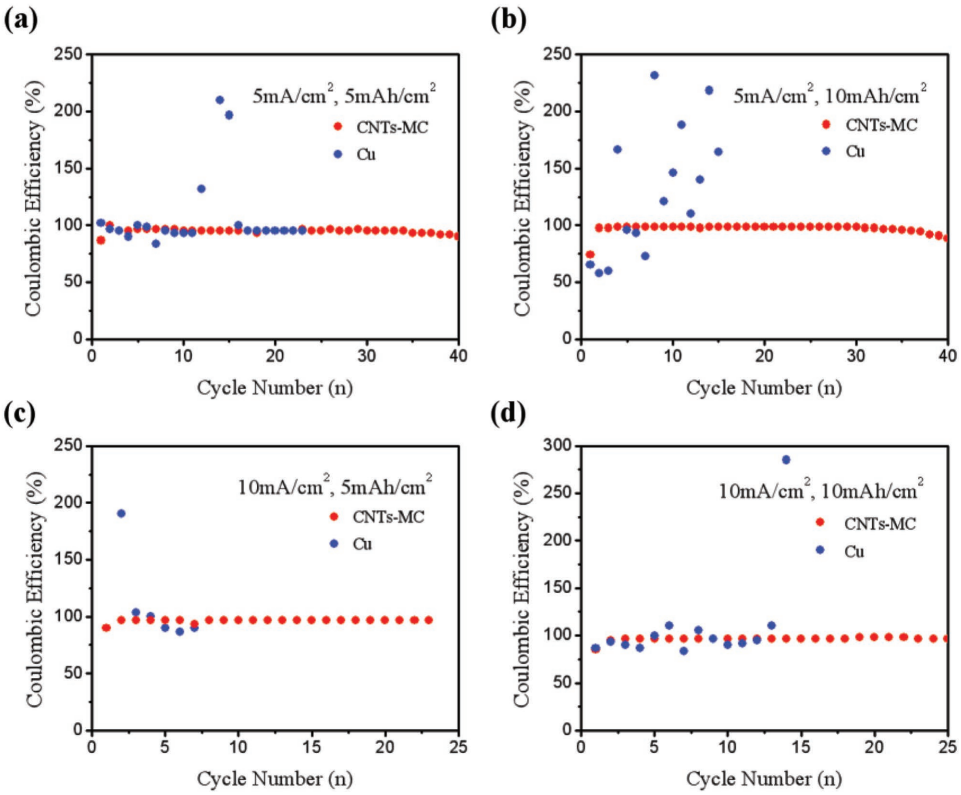

Figure 2. Coulombic efficiency evaluation of Li@CNTs-MC and Li@Cu measured at a) 5 mA cm^{-2} for 5 mA h cm^{-2}, b) 5 mA cm^{-2} for 10 mA h cm^{-2}, c) 10 mA cm^{-2} for 5 mA h cm^{-2}, and d) 10 mA cm^{-2} for 10 mA h cm^{-2} in Li plating. All the Li stripping was performed at the indicated plating current density till a cell voltage of 1 V.

or 40th cycles, respectively. A similar test on the Cu foil shows a large variation in Coulombic efficiency with cycles. When the electroplating duration was increased to 2 h for the same current of 5 mA cm^{-2}, a Li content of 42.5 wt% and a specific capacity of 1640 mA h g^{-1} are achieved. The corresponding Coulombic efficiency of CNTs-MC (Figure 2b) is 74.2%, 98.3%, 98.3%, or 95.8% for the 1st, 5th, 20th, or 35th cycles, respectively. More impressively, when the plating was performed at a current of 10 mA cm^{-2}, high Coulombic efficiency values are maintained for both 0.5 h (90% and 96.7% for the 1st and 20th cycles, Figure 2c) and 1 h (85% and 96.7% for the 1st and 25th cycles, Figure 2d) plating durations. The CNTs-MC remains stable at hush plating/stripping conditions, showing an outstanding reversibility and high Li utilization as a Li anode. In contrast, the commercial Cu foils display unsatisfactory Coulombic efficiency at the high areal capacity (≥5 mA h cm^{-2}) and the high current density (≥5 mA cm^{-2}), in which the formation[26] and fracture of Li dendrite[24] may induce the fluctuation. The composition of SEI on CNTs-MC after the 1st plating and the 10th plating for a capacity of 10 mA h cm^{-2} plated at 10 mA cm^{-2} has been investigated by XPS. As shown in Figure S6 (Supporting Information), after the 1st plating, components of ROLi, ROCOOLi, and LiF are observed on the surface of CNTs-MC, consistent to previous report.[23] The SEI composition after 10 cycles does not show much change, indicating the excellent stability of SEI layer during cycling, which is beneficial to reduce the loss of Li/electrolyte and to maintain the Coulombic efficiency.

To evaluate the cycling performance of the CNTs-MC anode, the voltage variation has been monitored during the Li plating/stripping in half cells. **Figure 3**a shows the voltage profiles of Li@CNTs-MC and Li@Cu at 5 mA cm^{-2} for a capacity of 5 mA h cm^{-2}. Li@CNTs-MC exhibits a low overpotential of ≈60 mV till 160 h, while the Li@Cu shows much larger overpotential with remarkable fluctuations and eventually an internal short circuit after 100 h. A similar voltage profile (Figure 3b) has been obtained from CNTs-MC with a cycling life of 600 h at 5 mA cm^{-2} for 10 mA h cm^{-2}, while the Cu foil shows a short circuit in 100 h under the same conditions. When the current density is increased to 10 mA cm^{-2} for a plating/striping duration of 0.5 h (corresponding to a capacity of 5 mA h cm^{-2}), the voltage of Li@Cu behaves like a random oscillation, while the Li@CNTs-MC remains a low overpotential of ≈100 mV for 300 h (Figure 3c). When tested under the same condition in Figure 3b,c, the bare MC without CNTs shows fluctuant voltages with much larger overpotentials (>500 mV) and an internal short circuit occurs after 150 h (Figure S7, Supporting Information), indicating that CNTs are critical to the superior cycling performance of CNTs-MC. The Li@CNTs-MC remains stable at 10 mA cm^{-2} for a plating/striping duration of 1 h (leading to a capacity of 10 mA h cm^{-2}) for 180 h (Figure 3d). The overpotential augmentation observed in the initial several cycles could be attributed to the high yet unstable energy barrier during the formation of SEI[27] and the interface between Li and the electrode, which will be discussed in detail later. More impressively, when the current density is further increased to 15 mA cm^{-2} for a capacity of 15 mA h cm^{-2}, the Li@CNTs-MC displays a fluctuating voltage in the first 300 h (Figure S8, Supporting Information), but is still cyclable in the second 300 h.

The SEI on CNTs-MC for 15 mA h cm^{-2} plated at 15 mA cm^{-2} has been checked by XPS, as shown in Figure S9 (Supporting Information). We can see that the amount of ROCOOLi and LiF is increased after 10 cycles, as a result of repeated growth/corrosion of SEI.[23] Among the various components in SEI, the

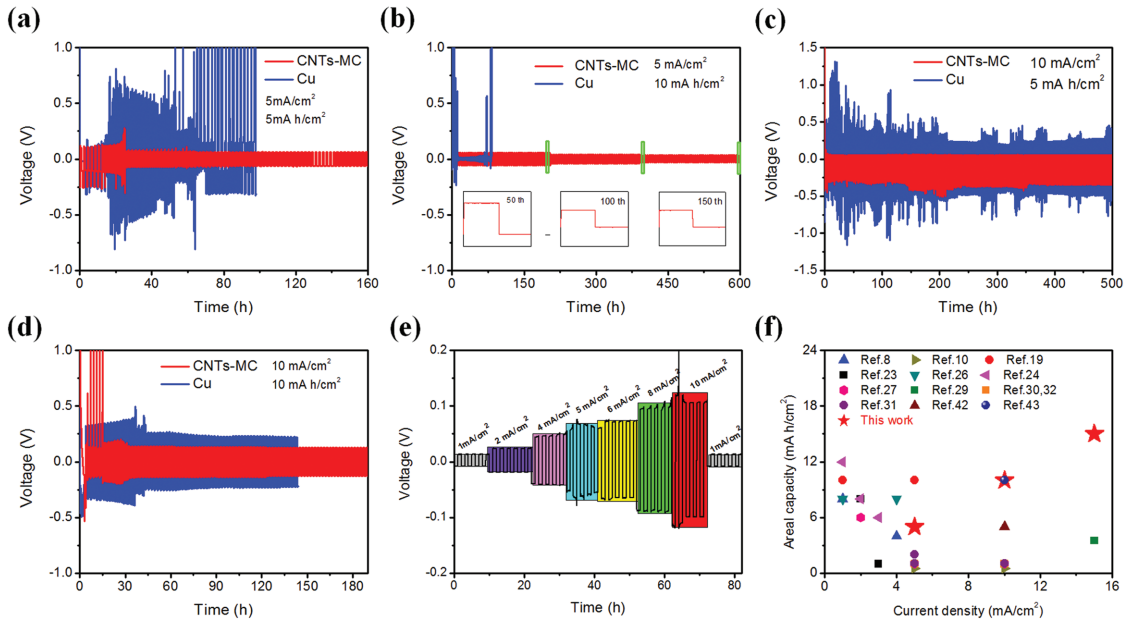

Figure 3. Voltage profiles of Li plating/stripping on CNTs-MC and Cu. a) 5 mA cm^{-2} for 5 mA h cm^{-2} with Li utilization of ≈62.5%, b) 5 mA cm^{-2} for 10 mA h cm^{-2} with Li utilization of ≈100%. Inset shows Li plating/stripping voltage profiles of the 50th, 100th, and 150th cycles, respectively. c) 10 mA cm^{-2} for 5 mA h cm^{-2} with Li utilization of ≈62.5%. d) 10 mA cm^{-2} for 10 mA h cm^{-2} with Li utilization of ≈76.9%. e) Rate performance of Li@CNTs-MC measured at currents of 1, 2, 4, 5, 6, 8, and 10 mA cm^{-2} for 1 h in Li-stripping and Li-plating for each cycle. f) Comparison of CNTs-MC with some recently reported results showing the excellent cycle performances at high current density or high areal capacity.

organic ROCOOLi seems more electrochemically stable than the inorganic phases, which may significantly decrease the Li transport and increase the voltage.[38] The formation of SEI on CNTs-MC was also investigated by cyclic voltammogram (CV), as revealed by the irreversible cathodic peak at ≈1.7 V (Figure S10, Supporting Information).[39] The broad cathodic peak in the voltage range of 0–0.5 V, the reduction peak at ≈–0.1 V, the anodic peak at ≈0.07 V and the broad anodic peak between 0.15–0.5 V, correspond to the Li insertion in CNTs-MC,[40] metallic Li plating, metallic Li stripping[8] and Li extraction,[41] respectively. By integrating the CV curves, the capacity corresponding to above-mentioned processes were estimated in Table S1 (Supporting Information). As can be seen, the irreversible Li consumption is ≈1.75 mA h cm^{-2}, including ≈1.366 mA h cm^{-2} for the formation of SEI and ≈0.384 mA h cm^{-2} of other Li loss during the insertion/extraction process. In principle, a prelithiation of 3 mA h cm^{-2} is able to compensate all the irreversible Li consumption.

The rate performance of CNTs-MC (Figure 3e) was evaluated by cycling the cell at different currents with each for 1 h. For the currents of 1, 2, 4, 5, 6, 8, and 10 mA cm^{-2}, the overpotential is 12, 25, 45, 60, 70, 90, and 100 mV, respectively. The relatively low overpotentials at high currents indicate the fast kinetics of Li^+ migration and the superior interface properties,[18,19,23] which could be further proved by electrochemical impedance spectroscopy (EIS) data (Figure S11, Supporting Information). The semicircle at the high frequency range in the Nyquist plots indicates the interfacial resistance through SEI and that at the low frequency range indicates the charge-transfer resistance at the Li metal surface.[22] By fitting the EIS curves, the resistances were estimated and are listed in Table S2. As can be seen, the Li@CNTs-MC cell displays an interfacial impedance of 92.4 Ω, lower than 98.2 Ω for Li@Cu before cycling; after one cycle, the Li@CNTs-MC cell displays an interfacial impedance of 17.7 Ω, slightly lower than 18.7 Ω for Li@Cu. The cycling performance of CNTs-MC is comparable or superior to previous reports in terms of working current and areal capacity (Figure 3f, Table S3, Supporting Information).[8,10,19,23,24,26–32,42,43] Most Li-metal anodes reported are limited by the charging/discharging current of ≤5 mA cm^{-2} (for capacities ≥5 mA h cm^{-2})[8,23,24,26] and the capacity of ≤ 5 mA h cm^{-2} (for current ≥5 mA cm^{-2}).[10,27–32] Full cells with Li@CNTs-MC as anode and $LiFePO_4$ (mass loading of ≈3.0 mg cm^{-2} on Al foil) as cathode were assembled and tested to show the potential advantage of Li@CNTs-MC in practical applications. As can be seen from Figure S12 (Supporting Information), the full cell of Li@CNTs-MC/$LiFePO_4$ delivers a specific capacity of 143 mA h g^{-1} (with respect to the mass of $LiFePO_4$) with a Coulombic efficiency of 94.5% in the first cycle, and retains a capacity of 140 mA h g^{-1} with a Coulombic efficiency of 98.3% after 70 cycles of testing at 0.5 C; the performance is comparable or superior to previous reports.[19,23,31] Under the same conditions, the cell assembled with Li foil as the anode delivers a specific capacity of 146 mA h g^{-1} in the first cycle and drops to 107 mA h g^{-1} with a Coulombic efficiency of 42.7% after 40 cycles.

To further understand the mechanisms for the excellent performance of CNTs-MC at high currents and capacities, the morphological evolution of CNTs-MC during Li plating/stripping has been investigated and shown in **Figure 4**a. When Li is pre-electroplated at 1 mA cm^{-2} for 3 h, the Li prefers to deposit on the tips of CNTs in CNTs-MC, forming numerous protrusions (Stage A). The TEM mapping (Figure S13, Supporting Information) clearly shows the existence of Ni and C in the protrusions. After 10 mA h cm^{-2} Li is plated on CNTs-MC at a current of 10 mA cm^{-2}, Li particles with smooth surface uniformly emerge on the CNTs-MC without recognizable Li dendrites (Stage B). In contrast, under the same plating conditions on Cu, dendrites are observed (Figure S15, Supporting Information). When 10 mA h cm^{-2} of Li is stripped at 10 mA cm^{-2} in the 1st cycle, the structure of CNTs-MC is maintained (Figure S14 c, Supporting Information) and the surface of CNTs-MC shows honeycomb-like structure with nanowalls (Stage C), probably related to the strong interaction between Li and CNTs. The development of such honeycomb-like structures is evidenced after the 4th (stage D) and 10th (stage E) stripping. Such a morphological evolution on CNTs-MC is more clearly illustrated by the schematic in Figure 4b. In the Li preplating process, Li nanoparticles are uniformly deposited on the CNTs due to the tip effects of CNTs[9] and the higher adsorption energy of Li on the curved CNTs.[36,44] The preferential presence of Li on CNTs would facilitate the Li deposition but hamper the Li stripping, which may explain the lower plating overpotential after the 1st cycle and high stripping overpotential in the initial several cycles observed previously. The subsequent plating fill up the space between CNTs and connects the CNTs together, forming Li particles but without dendrites due to the guidance of CNTs and N-doping effect in the carbon matrix.[20,23] In the Li stripping process, the strong interaction between Li and CNTs renders the Li on CNTs to be stripped more difficultly, leaving the nanowall-like structure. Such a network consisting of nanowalls provides the stable scaffold to host the Li plating in the subsequent cycles, generating a low local current to minimize the development of Li dendrites.

In the way described above, most strain generated in the Li plating/stripping has been neutralized by the CNTs and nanowalls, resulting less thickness change and higher cycling stability of the CNTs-MC electrode compared to bare Li on Cu. The measurements shown in Figure S14 (Supporting Information) indicate that the CNTs-MC electrode has thicknesses of ≈126.1 µm after the 1st plating, ≈99.7 µm after the 1st stripping and ≈128.9 µm after the 10th plating. The reversible thickness change of ≈29.3% is much smaller than 78.5% reported from pure CNT paper.[45] We demonstrate here that the introduction of flexible CNTs has increased the tolerance of the stiff MC scaffold to internal volume change. As shown in Figures 4c–e, CNTs-MC is elastic till a compressive strain of 80% (Figure 4 c) while bare MC is elastic only within a strain of 40% (Figure 4 d) and crashes for the strain of 80% (Figure 4 e). By integrating the compressive stress–strain curves, the internal friction and energy adsorption efficiency of MC and CNTs-MC were estimated and are listed in Table S4 (Supporting Information). Clearly, the internal friction and energy adsorption efficiency of CNTs-MC is higher than bare MC in the strain range of 0–40%, implying CNTs-MC has higher ability to relieve strain than MC due to the existence of CNTs. Therefore, the combination of stiff MC scaffold and flexible CNTs assures an overall small electrode thickness change but large internal adsorption ability to strains.

In summary, we have fabricated a Li-metal anode made of self-grown carbon nanotubes in melamine sponges

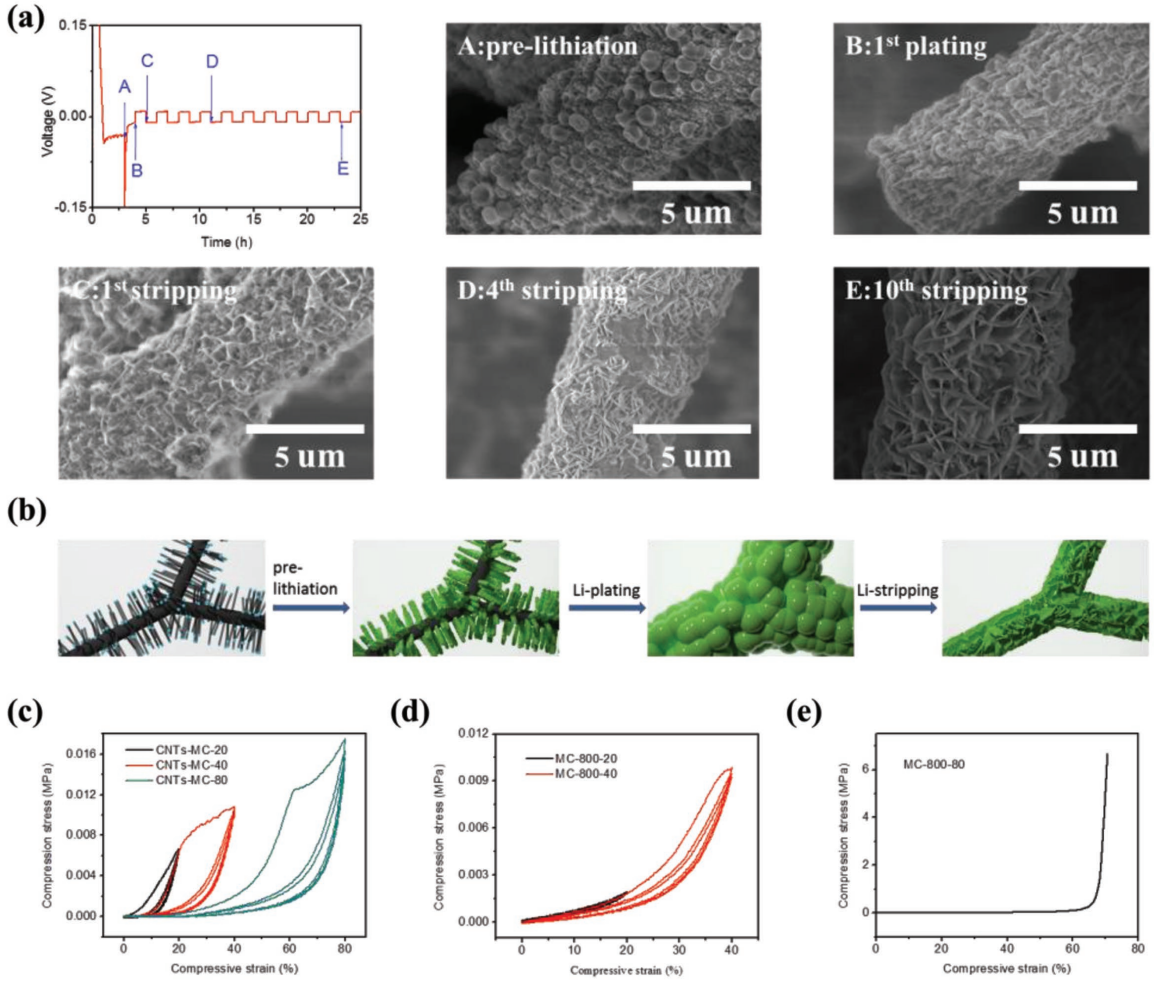

Figure 4. a) Voltage profile and morphological evolution on the CNTs-MC during the Li plating/stripping cycles. Stage A: after prelithiation at 1 mA cm^{-2} for 3 mA h cm^{-2}; Stage B: after the 1st Li plating at 10 mA cm^{-2} for 10 mA h cm^{-2}; Stage C: after the 1st Li stripping at 10 mA cm^{-2} for 10 mA h cm^{-2}; Stage D: after the 4th Li stripping at 10 mA cm^{-2} for 10 mA h cm^{-2}; Stage E: after the 10th Li stripping at 10 mA cm^{-2} for 10 mA h cm^{-2}. b) Schematic showing the morphological changes on the CNTs-MC in Li plating/stripping. c) Compression test for CNTs-MC with the strain varying from 0 to 20%, 0 to 40%, and 0 to 80%, respectively. Compression test for MC with the strain d) from 0% to 20% and 0% to 40%, and e) from 0% to 80%.

demonstrating high areal capacity of 15 mA h cm^{-2} cyclable at high current density of 15 mA cm^{-2}. The superior electrochemical performance is attributed to superior interface properties due to the conductive yet dendritic framework and the N and O-containing functional groups, greatly reducing the current density and guiding the homogenous Li growth with small nucleation overpotential. The combination of stiff scaffold and flexible CNTs assure a small reversible electrode thickness change while large ability of adsorption to strains during Li plating/stripping, resulting to an excellent structural stability in cycling. The rational design of the 3D carbons may shed light on further research in Li-metal anode and promote the realization of high-performance Li metal batteries.

Supporting Information

Supporting Information is available from the Wiley Online Library or from the author.

Acknowledgements

This work was supported by Natural Science Foundation of China (51772282) and funding from Hefei Center for Physical Science and Technology.

Conflict of Interest

The authors declare no conflict of interest.

Keywords

carbon nanotubes, high current, lithium-metal anodes, ultrahigh capacity

Received: August 31, 2018
Revised: November 19, 2018
Published online:

[1] W. Xu, J. Wang, F. Ding, X. Chen, E. Nasybulin, Y. Zhang, J. G. Zhang, *Energy Environ. Sci.* **2014**, *7*, 513.
[2] H. Kim, G. Jeong, Y. U. Kim, J. H. Kim, C.-M. Park, H.-J. Sohn, *Chem. Soc. Rev.* **2013**, *42*, 9011.
[3] D. Lin, Y. Liu, Y. Cui, *Nat. Nanotechnol.* **2017**, *12*, 194.
[4] P. G. Bruce, S. A. Freunberger, L. J. Hardwick, J. M. Tarascon, *Nat. Mater.* **2012**, *11*, 19.
[5] R. Bhattacharyya, B. Key, H. Chen, A. S. Best, A. F. Hollenkamp, C. P. Grey, *Nat. Mater.* **2010**, *9*, 504.
[6] K. J. Harry, D. T. Hallinan, D. Y. Parkinson, A. A. MacDowell, N. P. Balsara, *Nat. Mater.* **2014**, *13*, 69.
[7] F. Ding, W. Xu, G. L. Graff, J. Zhang, M. L. Sushko, X. Chen, Y. Shao, M. H. Engelhard, Z. Nie, J. Xiao, *J. Am. Chem. Soc.* **2013**, *135*, 4450.
[8] T. T. Zuo, X. W. Wu, C. P. Yang, Y. X. Yin, H. Ye, N. W. Li, Y. G. Guo, *Adv. Mater.* **2017**, *29*, 1700389.
[9] L. Enze, *J. Phys. D: Appl. Phys.* **1987**, *20*, 1609.
[10] X. B. Cheng, T. Z. Hou, R. Zhang, H. J. Peng, C. Z. Zhao, J. Q. Huang, Q. Zhang, *Adv. Mater.* **2016**, *28*, 2888.
[11] J. Qian, W. A. Henderson, W. Xu, P. Bhattacharya, M. Engelhard, O. Borodin, J. G. Zhang, *Nat. Commun.* **2015**, *6*, 6362.
[12] L. Suo, Y. S. Hu, H. Li, M. Armand, L. Chen, *Nat. Commun.* **2013**, *4*, 1481.
[13] W. Li, H. Yao, K. Yan, G. Zheng, Z. Liang, Y. M. Chiang, Y. Cui, *Nat. Commun.* **2015**, *6*, 7436.
[14] X. Han, Y. Gong, K. K. Fu, X. He, G. T. Hitz, J. Dai, A. Pearse, B. Liu, H. Wang, G. Rubloff, *Nat. Mater.* **2017**, *16*, 572.
[15] Y. Lu, Z. Tu, L. A. Archer, *Nat. Mater.* **2014**, *13*, 961.
[16] G. Zheng, S. W. Lee, Z. Liang, H. W. Lee, K. Yan, H. Yao, H. Wang, W. Li, S. Chu, Y. Cui, *Nat. Nanotechnol.* **2014**, *9*, 618.
[17] N. W. Li, Y. X. Yin, C. P. Yang, Y. G. Guo, *Adv. Mater.* **2016**, *28*, 1853.
[18] S. Jin, S. Xin, L. Wang, Z. Du, L. Cao, J. Chen, X. Kong, M. Gong, J. Lu, Y. Zhu, *Adv. Mater.* **2016**, *28*, 9094.
[19] S. Jin, Z. Sun, Y. Guo, Z. Qi, C. Guo, X. Kong, Y. Zhu, H. Ji, *Adv. Mater.* **2017**, *29*, 783.
[20] R. Zhang, X. R. Chen, X. Chen, X. B. Cheng, X. Q. Zhang, C. Yan, Q. Zhang, *Angew. Chem., Int. Ed.* **2017**, *56*, 7764.
[21] K. Yan, Z. Lu, H. W. Lee, F. Xiong, P. C. Hsu, Y. Li, J. Zhao, S. Chu, Y. Cui, *Nat. Energy* **2016**, *1*, 16010.
[22] D. Lin, Y. Liu, Z. Liang, H. W. Lee, J. Sun, H. Wang, K. Yan, J. Xie, Y. Cui, *Nat. Nanotechnol.* **2016**, *11*, 626.
[23] L. Liu, Y. X. Yin, J. Y. Li, S. H. Wang, Y. G. Guo, L. J. Wan, *Adv. Mater.* **2018**, *30*, 6216.
[24] S. Liu, A. Wang, Q. Li, J. Wu, K. Chiou, J. Huang, J. Luo, *Joule* **2018**, *2*, 184.
[25] R. Zhang, N. W. Li, X. B. Cheng, Y. X. Yin, Q. Zhang, Y. G. Guo, *Adv. Sci.* **2017**, *4*, 1600445.
[26] H. Ye, S. Xin, Y. X. Yin, J. Y. Li, Y. G. Guo, L. J. Wan, *J. Am. Chem. Soc.* **2017**, *139*, 5916.
[27] D. Lin, J. Zhao, J. Sun, H. Yao, Y. Liu, K. Yan, Y. Cui, *Proc. Natl. Acad. Sci. USA* **2017**, 201619489.
[28] X. B. Cheng, H. J. Peng, J. Q. Huang, R. Zhang, C. Z. Zhao, Q. Zhang, *ACS Nano.* **2015**, *9*, 6373.
[29] C. Jin, O. Sheng, Y. Lu, J. Luo, H. Yuan, W. Zhang, H. Huang, Y. Gan, Y. Xia, C. Liang, J. Zhang, X. Tao, *Nano Energy* **2018**, *45*, 203.
[30] L. Fan, H. L. Zhuang, W. Zhang, Y. Fu, Z. Liao, Y. Lu, *Adv. Energy Mater.* **2018**, *8*, 1703360.
[31] W. Deng, X. Zhou, Q. Fang, Z. Liu, *Adv. Energy Mater.* **2018**, *8*, 1703152.
[32] W. Zhang, H. L. Zhuang, L. Fan, L. Gao, Y. Lu, *Sci. Adv.* **2018**, *4*, eaar4410.
[33] L. Hong, X. Xiaoxiong, *Energy Storage Sci. Technol.* **2016**, *5*, 607.
[34] G. Li, J. Sun, W. Hou, S. Jiang, Y. Huang, J. Geng, *Nat. Commun.* **2016**, *7*, 10601.
[35] A. C. Dupuis, *Prog. Mater. Sci.* **2005**, *50*, 929.
[36] Z. Tan, K. Ni, G. Chen, W. Zeng, Z. Tao, M. Ikram, Q. Zhang, H. Wang, L. Sun, X. Zhu, *Adv. Mater.* **2017**, *29*, 1603414.
[37] K. Xiao, L. X. Ding, G. Liu, H. Chen, S. Wang, H. Wang, *Adv. Mater.* **2016**, *28*, 5997.
[38] X. B. Cheng, R. Zhang, C. Z. Zhao, F. Wei, J. G. Zhang, Q. Zhang, *Adv. Sci.* **2016**, *3*, 1500213.
[39] S. J. An, J. Li, C. Daniel, D. Mohanty, S. Nagpure, D. L. Wood III, *Carbon* **2016**, *105*, 52.
[40] Z. Wang, D. Xu, H. Wang, Z. Wu, X. Zhang, *ACS Nano* **2013**, *7*, 2422.
[41] N. A. Kaskhedikar, J. Maier, *Adv. Mater.* **2009**, *21*, 2664.
[42] E. Cha, M. D. Patel, J. Park, J. Hwang, V. Prasad, K. Cho, W. Choi, *Nat. Nanotechnol.* **2018**, *13*, 337.
[43] R. Zhang, X. Chen, X. Shen, X. Q. Zhang, X. R. Chen, X. B. Cheng, C. Yan, C. Z. Zhao, Q. Zhang, *Joule* **2018**, *2*, 764.
[44] W. Koh, J. I. Choi, S. G. Lee, W. R. Lee, S. S. Jang, *Carbon* **2011**, *49*, 286.
[45] Z. Sun, S. Jin, H. Jin, Z. Du, Y. Zhu, A. Cao, H. Ji, L. J. Wan, *Adv. Mater.* **2018**, *30*, 1800884.